Science and Technology Infusion Climate Bulletin
NOAA's National Weather Service
36th NOAA Annual Climate Diagnostics and Prediction Workshop
Fort Worth, TX, 3-6 October 2011

Feasibility of Dynamical Seasonal Precipitation Prediction for the Pacific Islands

H. Annamalai[1], K.P. Sooraj[1], A. Kumar[2] and H. Wang[2]

[1]*IPRC/SOEST, University of Hawaii, Honolulu, HI*

[2]*Climate Prediction Center, NOAA/NWS/NCEP, Camp Springs, MD*

1. Introduction

With a substantial portion of the world's population influenced by climate variability, such as drought, flood, heat and cold waves, any capability to anticipate these fluctuations one or more seasons in advance would have measurable benefits for decision making in many sectors of society (Barnston *et al.* 2005). From the early 1980s to late 1990s, our ability to develop and improve coupled climate models have led to the ability to predict tropical climate variations with some success (Kang and Shukla 2006; Kirtman and Pirani 2009). Here, we examine the seasonal forecast performance of the National Centers for Environmental Prediction (NCEP) Coupled Forecast System (CFS) over the Tropics, and in particular, over the United States Affiliated Pacific Islands (USAPI).

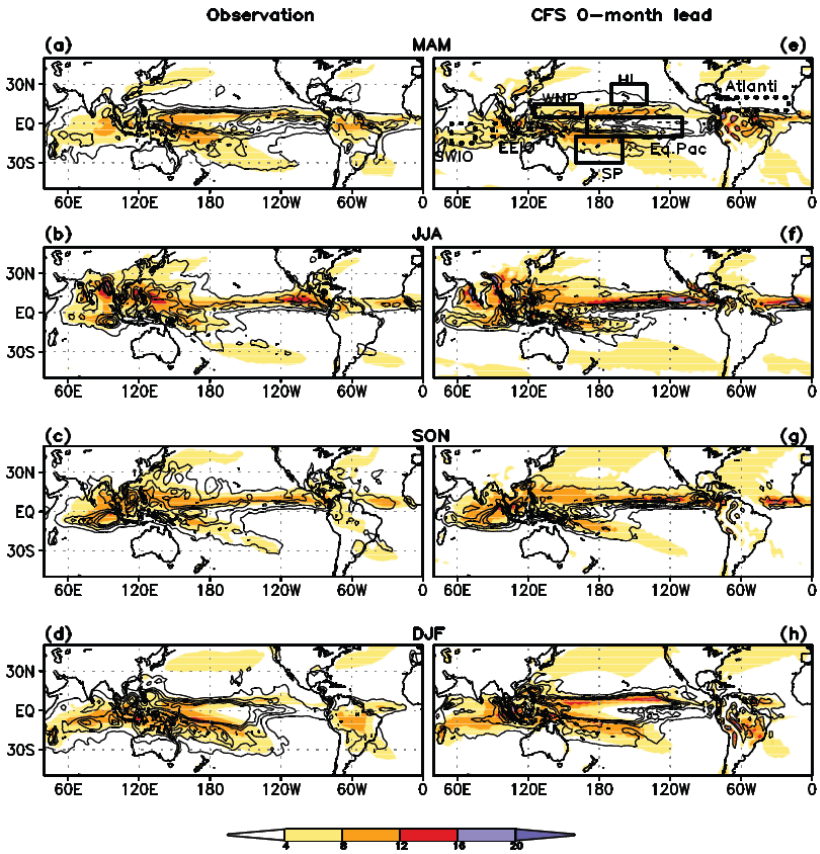

Fig. 1 Climatological precipitation (mm/day, shaded) and variance (mm^2/day, contours) for four standard seasons, (a-d) Observations and (e-h) 0-month CFS forecast. The boxed areas in (e) represent the regions where CFS ability in forecasting seasonal SST or precipitation anomalies are assessed. The area averaging used are: south west Indian Ocean (15°S-0°, 55°-75°E; SWIO); eastern equatorial Indian Ocean (10°S-0°, 90°-110°E; EEIO); northern Atlantic (20°-80°W, 10°-20°N) ; western north Pacific (5°-15°N, 125°-155°E; WNP); south Pacific (10°-30°S, 160°-200°E; SP); Hawaii (15°-30°N, 140°-170°W; HI), and equatorial Pacific (10°S-5°N, 170°-110°W; EPAC). Contours are drawn starting from 1 mm^2/day with an interval of 2 units.

Seasonal prediction over the tropics, and to a certain degree over the extratropics, is essentially linked to the accurate prediction of tropical SST (Shukla 1998; Kumar and Hoerling 1998; Goddard *et al.* 2001). Due to their impact on global climate anomalies (Ropelewski and Halpert 1987), predicting SST variations during the life cycle of El Niño–Southern Oscillation (ENSO) has been the focus of coupled model development. While efforts are underway to reduce model systematic errors, many Coupled General Circulation Models (CGCMs) have shown skill in capturing ENSO characteristics, paving ways for routine operational seasonal forecasts (Anderson *et al.* 2003; Saha *et al.* 2006). Recent studies have evaluated ENSO skills by analyzing hindcasts produced by CGCMs (Jin *et al.*

Correspondence to: H. Annamalai, International Pacific Research Center and School of Ocean and Earth Science and Technology, University of Hawaii, Honolulu, HI 96822; E-mail: hanna@hawaii.edu.

2008; Luo *et al.* 2008; Stockdale *et al.* 2011; Sooraj *et al.* 2011). Despite success, the predictive skills of models are degraded during the ENSO onset and decay periods (Barnston *et al.* 1999). Recent research interests have also focused on twotypes of El Niño namely, western Pacific and cold tongue events (*e.g.*, Kug *et al.* 2009).

While it is recognized that ENSO influences global climate anomalies, sensitivity experiments with AGCMs suggest that SST variations over the southwest Indian Ocean (SWIO) also modulate the amplitude of ENSO-induced circulation and precipitation anomalies over the tropical west Pacific (Watanabe and Jin 2003; Annamalai *et al.* 2005), and over the Pacific – North American (PNA) region (Annamalai *et al.* 2007). In summary, the expectation is that the combined effects of the tropical Pacific and Indian Oceans probably can further strengthen global climate anomalies.

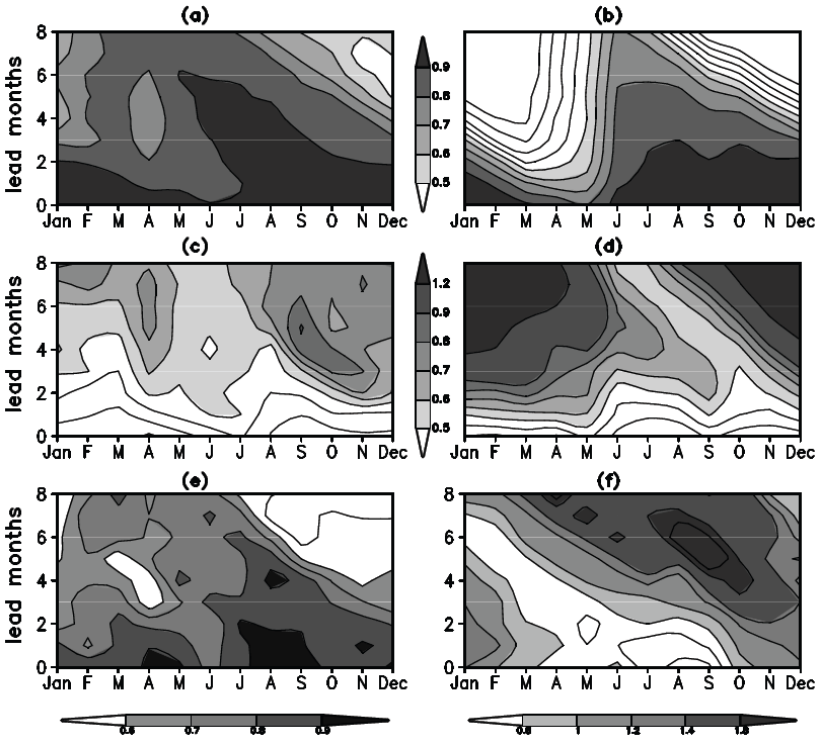

Fig. 2 (a) Anomaly correlation coefficient (ACC) of CFS ensemble mean forecasts of the monthly mean Nino3.4 SST over the period (1981-2005) as a function of initial condition month (x-axis) and lead months (y-axis). Nino3.4 is defined as the spatial mean SST over 5°S-5°N, 170°-120°W. (b) same as (a) but for persistence forecast. (c) same as (a) but for root mean square error (RMSE) for CFS ensemble forecast, and (d) same as (c) but for persistence forecast. (e) same as (a) but for CFS mean forecasts of the monthly mean precipitation anomalies over the equatorial Pacific (10°S-5°N, 170°E-110°W). (f) same as (c) but for monthly mean precipitation anomalies over the equatorial Pacific.

For the target regions over the USAPI (Fig. 1), the current operational seasonal precipitation prediction system is based on empirical methods in which SSTs provide the most reliable predictive information, and higher prediction skill is noticed during ENSO winters (He and Barnston 1996). During non-ENSO and weak to moderate ENSO events too, USAPI experience significant seasonal rainfall anomalies. In these circumstances, the precipitation forecast skill by empirical model is low, and the reasons may be manifold including: a) nonlinear relationship between ENSO SST and precipitation is not incorporated, b) details in the space-time evolution of SST during different flavors of ENSO are not properly accounted for, and c) SST anomalies other than ENSO may be responsible for rainfall variations. A prediction system based on a fully coupled dynamical model may overcome some of the above limitations.

2. Hindcasts and skill measures

Here, we analyze the output from CFS retrospective predictions (or alternatively referred to as hindcasts) that cover all 12 calendar months from 1981 to 2005. These hindcast runs, each of which is 9-month integration, are ensemble of 15 members starting from perturbed real-time oceanic and atmospheric initial conditions (ICs). Note that, for a 9-month integration, prediction at 6-month lead (L6) is the longest lead available for seasonal means while it is 8-month lead (L8) for prediction of monthly means. Variables examined in our analysis include SST, precipitation, and wind at 850 hPa. To infer the ocean Rossby waves in the tropical Indian Ocean (TIO), we also analyzed sea surface height (SSH). Hindcast anomalies are computed by removing the model climatology for each grid point, each initial month, and each lead time from the original ensemble hindcasts. Regarding verification of the real-time forecasts for the period 2006-09, we

examined 15-member ensemble members corresponding to the same ICs as in hindcasts. For the period 1981-2009, observed datasets used for verification include the CPC merged analysis of precipitation (CMAP) (Xie and Arkin 1996), winds from the NCEP/DOE reanalysis (Kanamitsu *et al.* 2002), and the NOAA optimally interpolated SST analysis (Reynolds *et al.* 2002). SSH is taken from the Global ocean data assimilation system. For verification observed data are interpolated to CFS' horizontal resolution (T62).

The entire range of available hindcasts (0 to 6 month lead) for all the four standard seasons is verified. To infer the uncertainty measures associated with forecasts, the skills are assessed using deterministic [anomaly correlation coefficient (ACC), the ensemble spread and signal-to-noise ratio (S/N)], categorical [Heidke skill score (HSS)], and probabilistic [rank probability skill score (RPSS)] methods. For the target regions (Fig. 1), the distribution of ensemble members, ensemble mean, and observed anomalies are plotted for every year. These plots aid in understanding year-to-year variations in the spread and its association with predicted value, and if there is asymmetry in model's predictive skill (positive *vs* negative values). More details are in Sooraj *et al.* (2011).

(a) Niño 3.4 region

Lead Months	DJF		MAM		JJA		SON	
	ACC	S/N	ACC	S/N	ACC	S/N	ACC	S/N
0	0.96	6.1	0.95	4.8	0.92	3.2	0.96	3.7
1	0.92	5.2	0.91	3.0	0.82	2.6	0.93	3.2
2	0.92	4.5	0.85	2.9	0.88	2.2	0.92	3.3
3	0.94	3.6	0.84	2.9	0.82	2.0	0.88	2.5
4	0.91	3.2	0.84	2.9	0.68	1.4	0.76	2.2
5	0.91	2.8	0.81	2.9	0.50	1.5	0.85	2.0
6	0.89	2.3	0.83	2.5	0.53	1.8	0.79	2.0

(b) SWIO region

Lead Months	DJF		MAM		JJA		SON	
	ACC	S/N	ACC	S/N	ACC	S/N	ACC	S/N
0	0.85	1.7	0.92	1.8	0.64	1.7	0.73	1.9
1	0.84	1.7	0.87	1.6	0.57	1.2	0.60	1.3
2	0.85	1.5	0.84	1.4	0.52	1.1	0.47	1.3
3	0.82	1.4	0.85	1.5	0.50	0.9	0.42	1.1
4	0.81	1.3	0.83	1.4	0.58	1.2	0.27	1.1
5	0.75	1.1	0.85	1.5	0.57	1.0	0.13	1.1
6	0.71	1.1	0.83	1.4	0.67	1.0	0.10	0.8

(c) EEIO region

Lead Months	DJF		MAM		JJA		SON	
	ACC	S/N	ACC	S/N	ACC	S/N	ACC	S/N
0	0.76	1.2	0.87	1.3	0.80	1.5	0.89	1.2
1	0.61	1.0	0.80	1.0	0.73	1.3	0.76	1.0
2	0.40	1.0	0.75	1.0	0.18	0.9	0.59	1.0
3	0.29	1.0	0.77	1.0	0.03	0.7	0.71	1.0
4	0.46	0.9	0.71	0.8	-0.04	0.4	0.51	0.9
5	0.48	0.9	0.67	0.9	-0.3	0.5	0.18	0.9
6	0.38	0.8	0.72	0.9	-0.1	0.5	0.04	0.8

Table 1 Values of anomaly correlation coefficient (ACC) and signal to noise ratio (SN) estimated for regional SST time series for four standard seasons, and for 0-6 month lead forecast.

3. Hindcast skills

Figure 1 shows climatological precipitation (shaded) and variance (contours) for standard seasons from observations (left) and at 0-month lead hindcast from CFS (right). Compared to observations, CFS captures the seasonal dependency in the position and intensity of the rainfall maximum and also regional variance maxima over the tropics with some systematic errors. Motivated by this, apart from examining SST skill, we also evaluate CFS' ability in forecasting: (i) tropical and regional precipitation anomalies; (ii) different flavors of El Niño and their associated regional response; and (iii) teleconnection between the tropical Pacific and Indian Ocean (TIO). In terms of regional indices, skill is examined for precipitation (area outlined in solid lines in Fig. 1), and SST influenced by thermocline variations over the TIO (area outlined in dotted lines in Fig. 1).

a. SST over the equatorial Pacific

Figure 2 shows ACC (Fig. 2a) and RMSE (Fig. 2c) for Niño3.4 SST anomalies estimated for the entire period. Results are shown for all lead times (0-8 months), and for all ICs (January through December). The corresponding measures estimated for persistence as the forecast are shown in Figs. 2b and 2d. The inverse association between ACC and RMSE holds good, and ensemble mean offers higher skills than persistence.

For instance, for leads up to 6-7 months and hindcasts initialized during late spring through early fall (May through October), the ensemble mean ACC is > 0.8 with relatively small RMSE (0.3-0.4) but for persistence forecast the ACC drops below 0.6 with higher RMSE (~0.7-0.8). This means that skill in forecasting the intensification and peak amplitude of ENSO is indeed high. However, for forecasts initialized during winter (November through January), skill in hindcasting the transition phase of ENSO is modest at best. Specifically, both methods share similar ACC and RMSE values in the first 3-5 months (Figs. 2a-d), but they drop off rapidly during spring with a minimum in July. This decay in skill, often referred to as the spring predictability barrier, is common to most models (*e.g.*, Jin and Kinter 2009), and the forecast performance of CFS over Niño3.4 region is comparable to the new ECMWF S3 system (Stockdale *et al.* 2011).

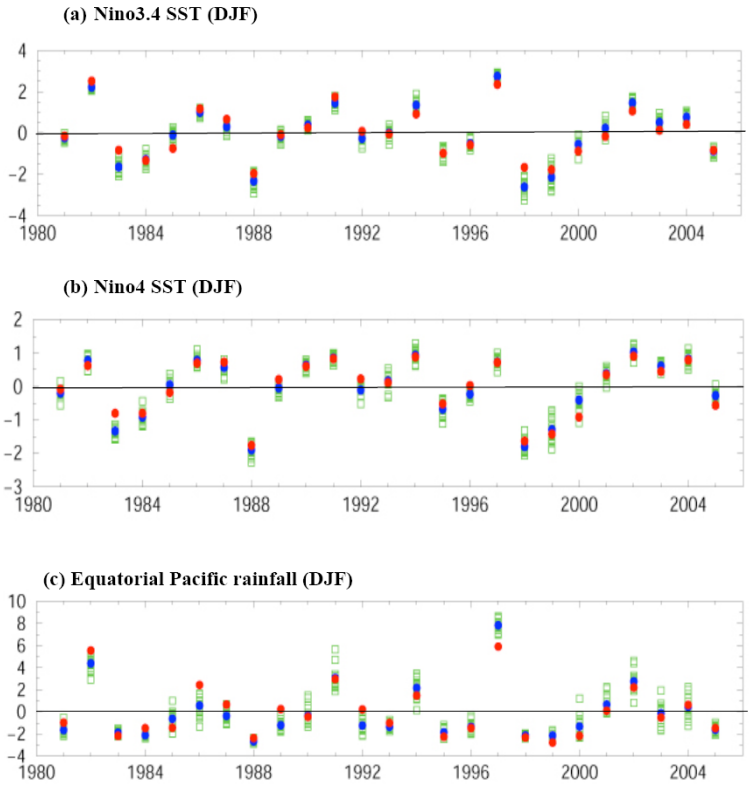

Fig. 3 (a-c) Temporal evolution of December through February average (DJF) SST anomalies (°C) hindcast by CFS at lead 0-month. Ensemble mean (blue), all 15 individual members (green) and observations (red) are shown for three regions: (a) Nino3.4 (5°S-5°N, 190°E-120°W); (b) Niño4 (5°S-5°N, 160°E-150°W); (c) same as (a) but for equatorial Pacific rainfall anomalies (mm/day) averaged over (10°S-5°N, 170°E-110°W).

ENSO prediction is further assessed in many different ways. First, the model's relative skill in hindcasting individual El Niño and La Nina events (Fig. 3a) is assessed for the peak phase (December through February; DJF) at 0-month lead. This is necessitated because observations during the period 1982-2005 indicate unique feature that models need to forecast. They include: (i) two of the strongest El Niño of the 20th century (1982 and 1997) and (ii) persistent La Nina during 1998-2000 (thick red circles in Fig. 3a). It is encouraging that all the ensemble members (green circles) capture correctly the amplitude during 1982 and 1997, and the model's ability in hindcasting these two events is remarkable even for leads up to 6 months (Sooraj *et al.* 2011). For the prolonged La Nina episode, however, the predicted amplitude is higher in conjunction with a larger ensemble spread. We also note that the model is able to correctly forecast near-normal conditions in many years. Second, we analyzed CFS' skill in forecasting different flavors of El Niño (Fig. 3b). Observations indicate that SST maximum for cold tongue events is over the eastern Pacific or Niño3 region (5°S-5°N, 90°W-150°W), and that for warm pool events the maixmum lies over the west-central Pacific or Niño4 region (5°S-5°N, 160°E-150°W). Therefore, skills in hindcasting SST anomalies over Niño3 and Niño4 regions are examined. Owing to the role of wave-induced thermocline displacements influening SST through vertical advection even at 6-month lead time, the ACC remains high (0.9) for Niño3 region and other skill measures are as good as that over the Niño3.4 region, and hence, are not discussed further. Over the Niño4 region, local warming during boreal winter of 1990-91; 1994-95; 2002-03 and 2004-05 are forecasted with a minimum spread (Fig. 3b). An examination for the entire period (not shown) suggests that prediction of SST anomalies over both Nino3 and Nino4 regions are comparable to those over Nino3.4 for all short leads. In summary, CFS' skill is higher for forecasting stronger and persisting El Niño events that are primarily due to thermocline displacements. When seasonally stratified, predicting winter and autumn seasonal SST anomalies have higher skill. However, forecasting weaker El Niño events is limited to 0-2 month leads.

b. Precipitation along the equatorial Pacific

The over-all skill measures for precipitation forecast along the equatorial Pacific (170°E-110°W; 10°S-5°N) are shown in Figs. 2e-f. High values of ACC (> 0.7) with less RMSE are along the diagonal representing fall and winter seasons. Only for short lead times (0-2 months), predicting spring and summer rainfall is skilful, and similar to SST, forecasting precipitation anomalies during ENSO phase transition is difficult. Encouraged by the skill in forecasting aspects of El Niño-related SST anomalies in individual years, we turn our attention to precipitation skill along the equatorial Pacific at 0-month lead for DJF season (Fig. 3c). While the ensemble mean follows the observed, the spread is larger yielding a S/N of about 4.2, and this skill is considerably less than that for Niño3.4 SST (Table 1a). Other limitations include excess rainfall during the winter of 1997/98, and the failure in capturing above normal rainfall during the winter of 1986-87. In addition, during cold phases of 1983-84 and 1998-99 (Fig. 3a), precipitation forecast is weaker than observed (Fig. 3c) despite predicting stronger SST anomalies compared to observations. SST anomalies translating into rainfall anomalies depends on physical parameterizations employed, particularly convective schemes. Further, SST-rainfall relationship is also not local, and rainfall anomalies can be influenced by circulation anomalies forced by rainfall at other locations.

(a) West Pacific region (125°-165°E, 5°N-15°N)

Lead Months	DJF		MAM		JJA		SON	
	ACC	S/N	ACC	S/N	ACC	S/N	ACC	S/N
0	0.87	2.3	0.66	1.7	0.66	1.2	0.31	0.8
1	0.77	1.9	0.63	1.2	0.69	1.1	-0.07	0.8
2	0.73	1.5	0.57	1.4	0.61	0.9	-0.06	0.6
3	0.84	1.7	0.54	1.5	0.69	0.8	-0.44	0.5
4	0.75	1.5	0.47	1.3	0.65	0.5	0.28	0.5
5	0.72	1.3	0.50	1.5	0.56	0.5	-0.07	0.4
6	0.58	1.3	0.53	1.5	0.22	0.5	-0.09	0.4

(b) South Pacific region (160°E-160°W, 10°S-30°S)

Lead Months	DJF		MAM		JJA		SON	
	ACC	S/N	ACC	S/N	ACC	S/N	ACC	S/N
0	0.69	2.0	0.72	1.7	0.56	1.8	0.72	1.7
1	0.69	1.9	0.75	1.4	0.46	1.4	0.62	1.7
2	0.63	1.6	0.72	1.5	0.32	1.2	0.62	1.4
3	0.56	1.4	0.65	1.5	0.32	1.2	0.52	1.3
4	0.51	1.2	0.67	1.2	0.44	1.0	0.39	1.1
5	0.41	1.0	0.74	1.6	0.22	1.0	0.49	1.0
6	0.35	1.0	0.71	1.4	0.37	1.2	0.48	1.0

(c) Hawaiian region (170°W-140°W, 15°N-30°N)

Lead Months	DJF		MAM		JJA		SON	
	ACC	S/N	ACC	S/N	ACC	S/N	ACC	S/N
0	0.62	1.1	0.69	1.5	0.57	1.4	0.49	0.9
1	0.69	1.0	0.44	1.3	0.69	1.1	0.44	1.0
2	0.60	0.9	0.52	1.3	0.62	1.1	0.32	0.9
3	0.57	0.9	0.49	1.1	0.64	1.1	0.22	0.8
4	0.34	0.7	0.46	1.2	0.46	0.8	0.39	0.7
5	0.27	0.6	0.34	1.3	0.55	0.9	0.12	0.6
6	0.14	0.6	0.49	1.0	0.61	0.9	0.34	0.7

Table 2 As in Table 1 but for regional precipitation time series over the Pacific Islands.

Finally, to depict coherency among variables responsible for ocean-atmosphere interactions, lagged correlations between DJF Niño3.4 SST and SST (contours), rainfall (shaded), and 850 hPa wind (vector) anomalies at lead 0 month and spanning the 24-month period (entire life-cycle of ENSO) are shown in Fig. 4b. Similar results from observations are also shown in Fig. 4a. In CFS, the onset, development, mature and decay stages of El Niño, as well as the development of cold SST and negative precipitation anomalies over the Maritime Continent (120°E-150°E) together with low-level divergence corresponding to anomalous Walker Circulation are in good agreement with observations. To the west of this center of divergence, easterly wind anomalies cover the entire equatorial Indian Ocean, and their influence on local ocean dynamics is explained next.

c. Teleconnection to the TIO

Figure 4c shows lagged correlations between DJF Niño3.4 time series and SSH (shaded) and SST (contours) averaged over (8°S-12°S) the TIO from observations, and the corresponding results from the 0-lead CFS forecast are shown in Fig. 4c. Starting from May-June of Year [0], upwelling- favourable winds off Java-Sumatra coasts (Figs. 4a-b; 80°E-100°E) promote negative SSH values (*i.e.*, shallow thermocline anomalies, Fig. 4d) and subsequent local SST cooling attains a maximum in fall (Figs. 4a-b). The wind-stress curl

associated with the easterly wind anomalies forces downwelling oceanic Rossby waves, and the westward tilted structure in SSH and SST anomalies with respect to time (Figs. 4c-d) support that interpretation. These Rossby waves advect warm water and act to deepen the thermocline as they cross the ocean basin (Xie *et al.* 2002). The maximum perturbation to SSH (*i.e.*, deepened thermocline) and SST are noted over SWIO during boreal spring of Year [+1]. The warm SST anomalies persist for about 10-12 months primarily due to the presence of shallow-mean thermocline and passage of oceanic Rossby waves. In summary, CFS captures the teleconnection from the tropical Pacific to TIO, and also the essential mechanisms responsible for the anomalous conditions in the TIO.

Encouraged by the above results, we examined skill scores over both SWIO (55°E-75°E; 15°S-0°), and EEIO (90°E-110°E, 10°S-0°). Observations indicate SST anomalies peak during spring of Year [+1] over SWIO and during boreal fall over EEIO, respectively. For SWIO, CFS hindcasts initialized from June-July of Year [0] onwards depicts higher ACC and lower RMSE than persistence method but in contrast, over EEIO ensemble mean barely does better than persistence even at shorter leads (Sooraj *et al.* 2011).

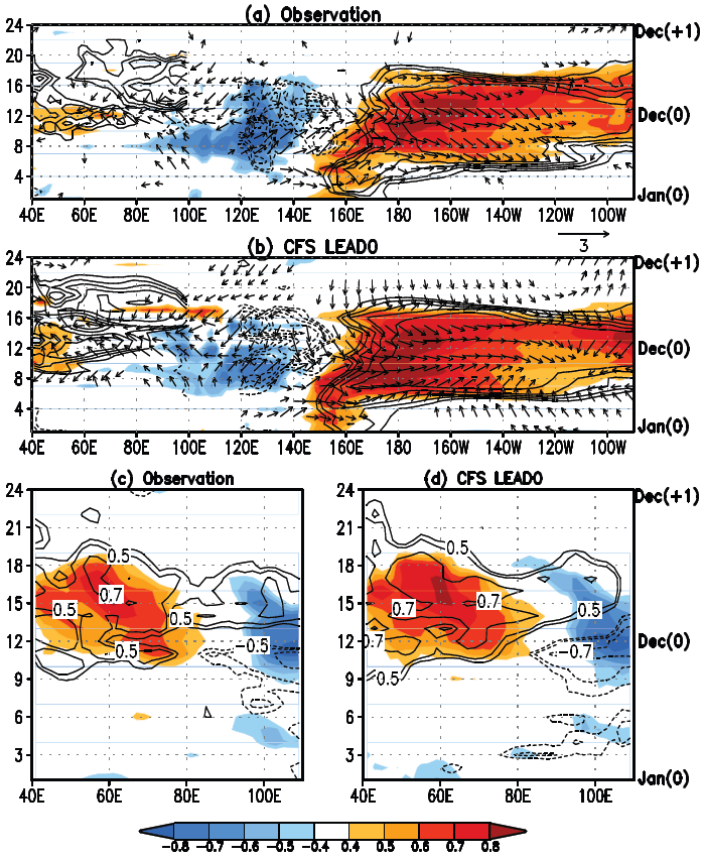

Fig. 4 (a) Lagged correlations of SST (contours), rainfall (shaded) and 850 hPa wind averaged in 3°S-3°N with winter (DJF) Nino3.4 SST index from observations. (b) same as (a) but from CFS ensemble mean 0-month lead forecast. Results are shown for a twoyear period representing the entire life-cycle of ENSO. (c) lagged correlations of SST (contours) and SSH (shaded) averaged in 8°-12°S with winter Nino3.4 SST index from observations. (d) same as (c) but from CFS ensemble mean 0-month lead forecast. Positive (negative) SST values are shown as solid (dashed) contours with an interval 0.1.

d. Precipitation over the USAPI

Figure 5 shows rainfall forecast over west Pacific islands (125°E-165°E; 5°N-15°N). The left (right) panels are results for 0-month (6-month) lead-time for standard seasons of summer (Figs. 5a-b), fall (Figs. 5c-d), winter (Figs. 5e-f) and spring (Figs. 5g-h). Observations (red circles) indicate that during strong El Niño years (*e.g.*, 1982-83; 1991-92; 1997-98), dryness (or below normal rainfall) persist from winter of Year [0] to summer of Year [+1]. Quite remarkably, CFS ensemble-mean forecast (blue circles) captures this drying tendency from 6-months lead time except for summer of Year [+1]. Barring the two strong El Niño events of 1982/83 and 1997/98, the spread among the ensemble members is large but the sign of the anomalies is well-captured. For 6-month lead forecast of JJA rainfall the predicted sign is wrong in many years. While correlations between rainfall anomalies over west Pacific and Nino3.4 SST anomalies is negative for most of the year, it is rather positive during July-August. Thus, the difficulty in capturing this seasonally-varying teleconnection may well be a factor in the low skill scores during summer. A possible interpretation is that large amplitude swings in precipitation occur during winter (Fig. 5e), and hence are more predictable.

Fig. 6 shows the results for the south Pacific islands (160°E-200°E; 10°S-30°S), and the skill statistics is summarized in Table 2b. In this region too, largest anomalies in precipitation are observed during ENSO winters (Figs. 6e-f) but the dryness starts in summer of Year [0] and persists until the following spring.

Interestingly, CFS correctly captures both the phase and amplitude of the dryness at longer lead times. However, for any given season ACC and S/N do not exceed 0.75 and 2.0, respectively. Compared to other seasons, forecasting rainfall anomalies during summer is less skilful (Table 2b) since ENSO teleconnection is weaker.

Another region of interest is the Hawaiian Archipelago (170°W-140°W; 15°N-30°N), and the precipitation forecasts are shown in Fig. 7 and the statistics are summarized in Table 2c. For the islands situated over the Northern Hemisphere, west Pacific and Hawaii, the dryness attains a maximum in winter of Year [0] and continues into the spring of Year [+1], and CFS has skill in forecasting them. However, the spread among the members is indeed large even during 1982-83 and 1997-98 El Niño years (Fig. 7) resulting in a low S/N (Table 2c). From Figs. 5-7 it is encouraging to note that observed anomalies (red dots), generally lie within the envelope of possible model solutions (green dots), and there are few instances of outliers.

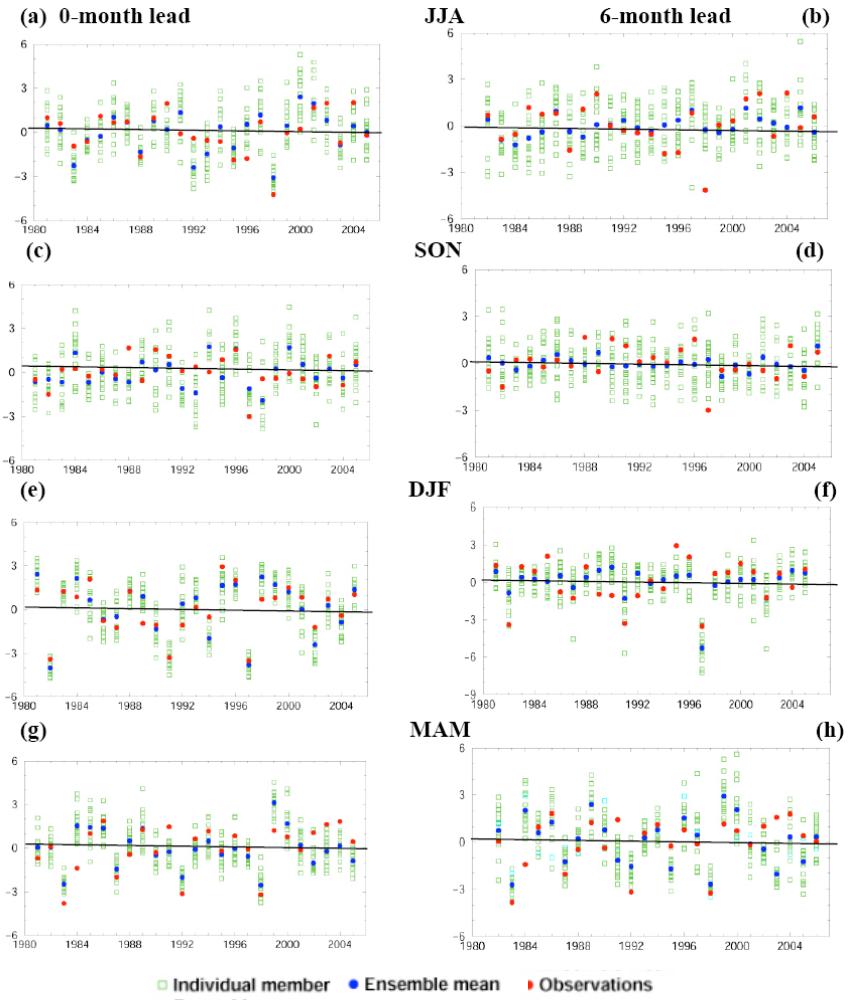

Fig. 5 Seasonal rainfall (mm/day) forecast at 0-month (left) and 6-month (right) lead time over tropical west north Pacific region for the period 1981-2005. Observations (red), ensemble-mean (blue) and all the 15 individual members (green) are shown.

4. Assessment of different aspects of forecasts

Here, ACC is compared and contrasted with HSS and RPSS to assess different aspects associated with forecasts that also rely on the spread information inherent in the ensembles (Kumar 2009). Our working hypothesis is that forecasts assessment based on ACC alone are perhaps not sufficient enough in the context of decision-making. As before, we assess the scores for SST indices (Fig.8). The left panels are scatter diagrams between ACC and HSS, while the right panels are scatter plots between ACC and RPSS, respectively.

CFS demonstrates highest confidence in predicting winter SST anomalies (open squares, Figs. 8a-b) over Niño3.4 region at all lead months with ACC upwards of 0.85. High skill in deterministic forecasts as measured by ACC is also captured for categorical and probabilistic forecasts with high HSS (> 50%) and RPSS (> 40%). This is consistent with the results discussed earlier (Fig. 2). The confidence in predicting fall season is also high but limited to 0-4 month leads. Predicting spring and summer anomalies has limited confidence at 0-1 month leads, and for other leads, even if ACC lies around 0.8, RPSS drops off to very low values sometimes even negative, indicating possible issues related to the spread among the ensemble members that influence the probabilistic forecasts. Therefore, forecasting the summer teleconnection features, *e.g.*, ENSO-monsoon association will be limited in CFS. The inference is that results of Fig. 2a and Table 1a

are encouraging, but additional diagnostics are necessary to attest the errors associated with the forecast for any decision-making.

For the SST indices over the TIO, the confidence in predicting the winter and spring variations over SWIO (Figs. 8c-d) are high at leads up to 5 months. Watanabe and Jin (2003) and Annamalai *et al.* (2005; 2007) noted that it is the winter and spring SST anomalies over SWIO that influence regional and global climate anomalies. In observations, summer and fall SST variations over SWIO are indeed small, and hence models have limited predictability. Confidence in predicting Indian Ocean Dipole Zonal Mode (IODZM) SST anomalies during fall is the least (Figs. 8e-f).

The scatter plots over the USAPI are shown in Fig. 9. Over the west Pacific region, forecasting rainfall variations during winter is trustworthy for at least 0-3 months lead, followed by prediction for spring season at lead 0-1 months. For summer rainfall variations, while ACC is greater than 0.6 and HSS around 15-25%, negative RPSS indicates that the forecast is not better than climatology. The model's forecast for fall rainfall anomalies is least skillful. A point to note here is that for the same value of ACC (~0.6) for 0-1 month lead forecast, RPSS is positive for spring but negative for summer indicating the seasonal dependency in the forecast errors. For the south Pacific region, predicting rainfall variations during winter and spring appear realistic for leads 0-4 months. Here also forecasting summer precipitation anomalies are not reliable. For the Hawaiian region, at shorter leads (0-1 months) and for all seasons except fall, convergence of all the three scores suggests that different rainfall forecast information are skilful and probably useful. In summary, for regional precipitation forecast over USAPI, ACC values greater than 0.7 and correspondingly high HSS and RPSS values occur particularly for winter and spring seasons.

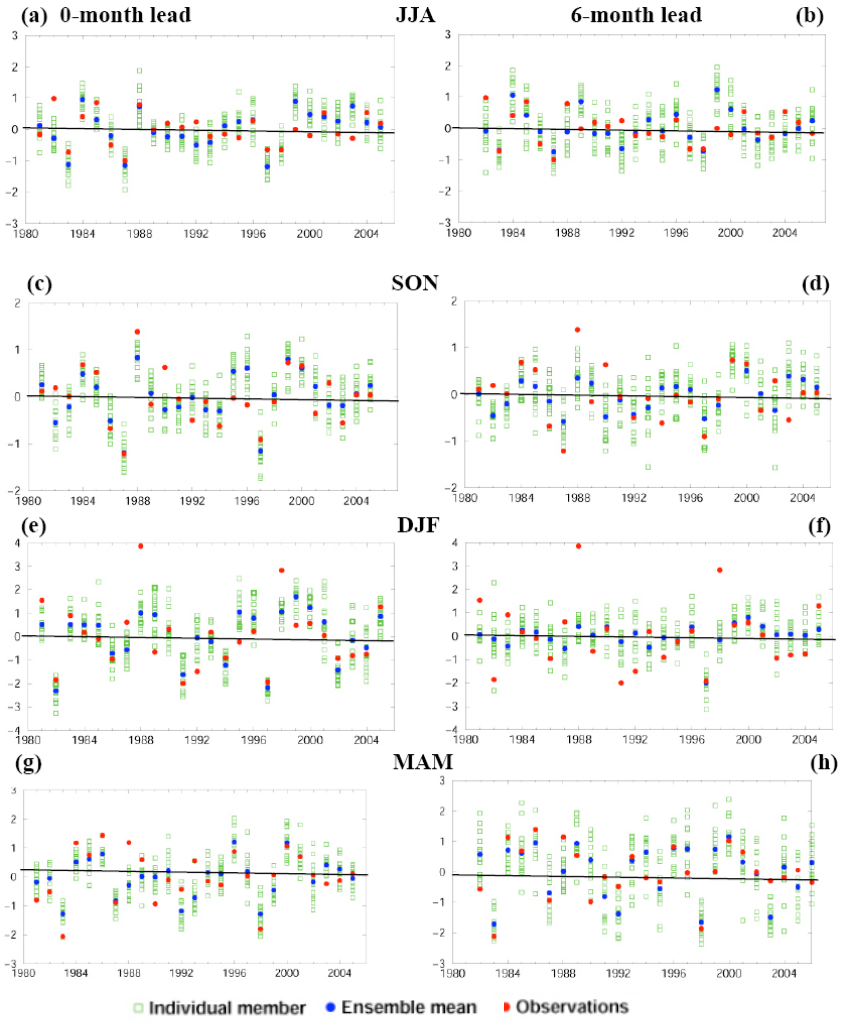

Fig. 6 Same as Fig. 5 but for the precipitation (mm/day) over south Pacific region.

5. Implications for dynamical seasonal prediction of precipitation

Both observational (Ropelewski and Halpert 1987; 1989) and modeling (*e.g.*, Shukla 1998; Su and Neelin 2002) studies provide a guide to the expected climatic impacts of ENSO over the tropics. The fact that an accurate prediction of the tropical Pacific SST is a necessary condition for successful prediction of rainfall along the equatorial Pacific is supported by the present analysis. Based on the lagged association between TIO and tropical Pacific SST anomalies, past seasonal prediction studies have used statistical methods to predict TIO SST anomalies (*e.g.*, Mason et *al.* 1999). However, recent studies also suggest that these ENSO-induced regional SST anomalies may possibly alter the strength of the circulation and rainfall anomalies elsewhere

(Annamalai *et al.* 2005; 2007). The ability of CFS in representing the coupled processes in the TIO, particularly over SWIO during ENSO years, deserves further attention.

Predictive skill of regional precipitation, however, is usually lower compared to SST and circulation (Kumar and Hoerling 1998) because of the "noisy", small-scale character, and complex physics of precipitation. Even averaged over a season substantial irregularities in the spatial pattern are likely, particularly over the Tropics where convective rainfall is most common (Gong *et al.* 2003). Even so, observational and modeling studies suggest that the large-scale circulation pattern responsible for the precipitation anomaly may be predictable several months in advance, particularly during ENSO events. An examination of spatial pattern of DJF SST and rainfall anomalies during all El Niño events indicate that CFS is capable of forecasting the "details", in particular the observed negative rainfall anomalies over all the three USAPI regions during 1982/93 and 1997/87, as well above normal rainfall over Hawaii during 1990-91, and 2004-05 events (figure not shown).

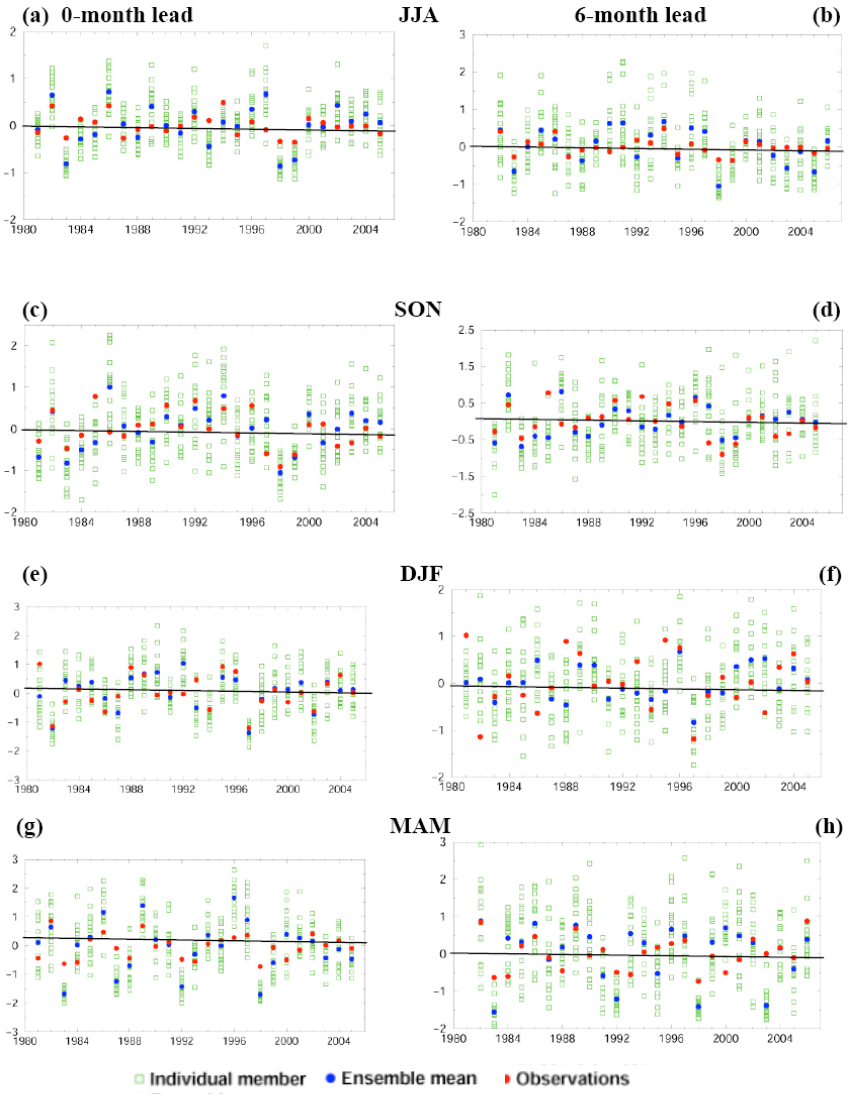

Fig. 7 Same as Fig. 5 but for the precipitation (mm/day) the Hawaii region.

Till date, the operational seasonal forecasting of precipitation over the USAPI stations relies on empirical method in which precipitation measured at individual stations itself is treated as a predictor (He and Barnston 1996). Their results based on the period 1955-94 suggest that at 1-month lead, ACC for predicting winter rainfall anomalies is ~ 0.4, 0.6, and 0.4 over south Pacific, west Pacific and Hawaiian regions, respectively (their Fig. 4). The dynamical forecast system based on CFS, on the other hand, demonstrates much higher skill at longer lead times over the USAPI (Table 2) when area-averaged fields are examined. Dynamical models represent the major components of the climate system (ocean, land and atmosphere) and can incorporate linear and nonlinear interaction processes among the components, and are expected to provide better seasonal forecasts than statistical models. A word of caution is that output from CFS represents averages over a relatively coarse grid, and therefore statistics of precipitation in regions of steep orography can differ substantially from that of station data. Nevertheless, owing to the success of CFS in forecasting the timing and amplitude of ENSO-related SST and precipitation anomalies along the equatorial Pacific and the associated teleconnection over the TIO we speculate that CFS has useful skill in forecasting regional rainfall anomalies over the USAPI. However, identifying individual physical processes responsible is beyond the scope of the present study. Lyon and Mason (2009) noted that the correct prediction of winter rainfall

anomalies during 1998 over southern Africa by some coupled models is probably not for the correct reasons. Our future study will examine the reasons for CFS performance over the USAPI.

6. Summary

The results presented here suggest the feasibility that a dynamical system based seasonal prediction of precipitation over the USAPI can be considered. It is necessary to continually assess the sources, and level of prediction skill as newer set of hindcasts based on improved models, and initial conditions obtained from more advanced data assimilation systems become available. For instance, one clear limitation in the hindcasts analyzed here is that for short-lead forecasts the initial conditions are from the old reanalysis system, a situation that would be rectified with the new CFS forecast model. In addition, in the updated CFS version the atmospheric model has a higher horizontal resolution (T126 compared to T62 in the current version), and may provide a better resolution necessary for precipitation prediction. In a future study, the physical processes that may be responsible for the performance of the model in predicting regional rainfall anomalies will also be examined. To attain station-level prediction of rainfall anomalies over the USAPI a downscaling system may need to be constructed.

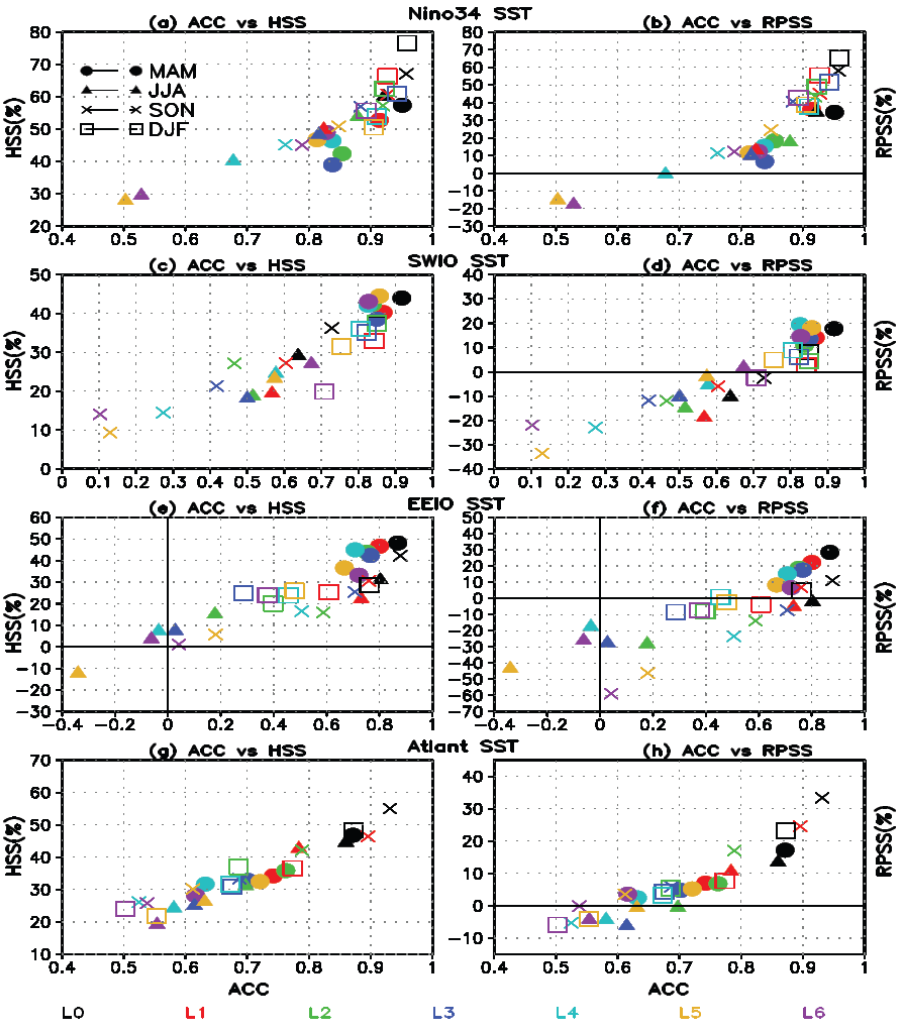

Fig. 8 Scatter diagram between ACC and HSS (left) and ACC and RPSS (right) for four standard seasons derived from CFS forecasts at 0-6 month leads; (a-b) for Nino3.4 SST, (c-d) SWIO SST, (e-f) EEIO SST indices and (g-h) Atlantic SST indices.

References

Anderson, D.L.T, and Coauthors 2003: Comparison of the ECMWF seasonal forecast system 1 and 2, including relative performance for the 1997/8 El Niño. Tech.Memo. **404**, ECMWF, Reading, UK, 93 pp.

Annamalai, H., P. Liu, and S.P. Xie, 2005: Southwest Indian Ocean SST variability: Its local effect and remote influence on Asian monsoons. *J. Climate,* **18,** 4150-4167.

—, H. Okajima, and M. Watanable., 2007: Possible impact of the Indian Ocean SST on the Northern Hemisphere circulation during El Niño. *J. Climate,* **20,** 3164-3189.

Barnston, A. G., M. H. Glantz, and Y. He., 1999: Predictive skill of statistical and dynamical climate models in SST forecasts during the 1997—98 El Niño episode and the 1998 La Niña onset. *Bull. Amer. Meteor. Soc.,* **80,** 217–244.

Barnston, A. G., A. Kumar, L. Goddard, and M. P. Hoerling, 2005: Improving seasonal prediction practices through attribution of climate variability. *Bull. Amer. Meteor. Soc.*, **86**, 59–72.

Goddard, L., S. J Mason, S. E. Zebiak, C. F. Ropelewski, R. Basher, and M. A. Cane, 2001: Current approaches to seasonal-to-interannual climate predictions. *Int. J. Climatol*, **21**, 1111-1152.

Gong, X., A.G. Barnston, and M.N. Ward, 2003: The effect of spatial aggregation on the skill of seasonal precipitation forecasts. *J. Climate,* **16,** 3059-3071.

He, Y., and A.G. Barnston, 1996: Long-lead forecasts of seasonal precipitation in the tropical Pacific islands using CCA. *J. Climate,* **9,** 2020-2035.

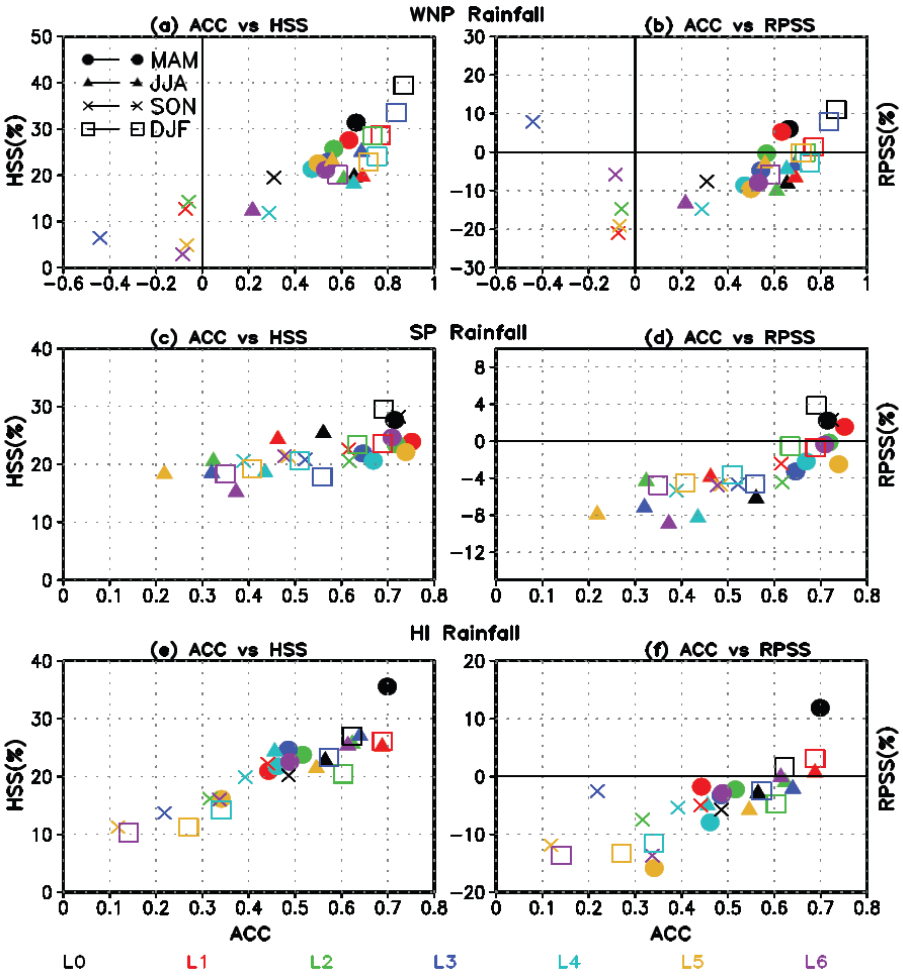

Fig. 9 Same as Fig. 8 but for regional precipitation indices; (a-b) west north Pacific, (c-d) south Pacific, and (e-f) Hawaii.

Jin, E. K, and J.L. Kinter, 2009: Characteristics of tropical Pacific SST predictability in coupled GCM forecasts using the NCEP CFS. *Climate Dyn*, **32,** doi, 10.1007/s00382-008-0418-2

Jin, E.K., and Coauthors 2008: Current status of ENSO prediction skill in coupled ocean-atmosphere models. *Climate Dyn,* **31**, 647–664.

Kanamitsu, M., W. Ebisuzaki, J. Woollen, S.-K. Yang, J.J. Hnilo, M. Fiorino, and G.L. Potter, 2002: NCEP-DOE AMIP-II Reanalysis (R-2), *Bull. Amer. Met. Soc.*, **83,** 1631-1643.

Kang, I-S., and J. Shukla, 2006: Dynamical seasonal prediction and predictability of the monsoon. B. Wang (Ed), The Asian Monsoon. Springer, 586-612.

Kirtman, B., and A. Pirani, 2009: The state of the Art of Seasonal Prediction: Outcomes and Recommendations from the First World Climate Research Program Workshop on Seasonal Prediction, *Bull. Amer. Meteor. Soc.*, **90,** 455-458.

Kug, J.S., F.F. Jin, and S.I. An., 2009: Two types of El Niño events: cold tongue El Niño and warm pool El Niño. *J. Climate,* **22,** 1499-1515.

Kumar, A., and M. P. Hoerling, 1998: Annual cycle of Pacific–North American predictability associated with different phases of ENSO. *J. Climate,* **11,** 3295–3308.

—, 2009: Finite samples and uncertainty estimates for skill measures for seasonal prediction, *Mon. Wea. Rev.*, **137,** 2622-2631.

Luo, J.J., S. Masson, S.K. Behera, and T. Yamagata, 2008: Extended ENSO predictions using a fully coupled ocean-atmosphere model. *J. Climate*, **21,** 84-93.

Lyon, B., and S. Mason, 2009: The 1997/98 summer rainfall season in southern Africa. Part II: Model simulations and coupled model forecasts. *J. Climate,* **22**, 3802-3818.

Mason S J, L Goddard, N E Graham, E Yulaeva, L Sun and P A Arkin, 1999: The IRI seasonal climate prediction system and the 1997/98 El Niño event, *Bull. Amer. Meteor. Soc.,* **80,** 1853-1873.

Reynolds, R. W., N. A. Rayner, T. M. Smith, D. C. Stokes and W. Wang, 2002, An improved in situ and satellite SST analysis for climate. *J. Climate*, **15,** 1609-1625.

Ropelewski, C. F and M.S. Halpert, 1987: Global and regional scale precipitation associated with El Niño/Southern Oscillation, *Mon. Wea. Rev.*, **115,** 1606-1626.

—, and —, 1989: Precipitation pattern associated with the high index phase of the Southern Oscillation. *J. Climate*, **2,** 268-284.

Saha S., and Coauthors 2006: The NCEP climate forecast system. *J. Climate,* **19,** 3483-3517.

Shukla J., 1998: Predictability in the midst of chaos: A scientific basis for climate forecasting. *Science,* **282,** 728–731.

Sooraj, K.P., H. Annamalai, A. Kumar and H. Wang, 2011: A comprehensive assessment of CFS seasonal forecasts over the Tropics. *Weather and Forecasting*, (in press).

Stockdale, T.N., D.L. Anderson, M.A. Balmaseda, F.D. Reyes, L. Ferranti, K. Mogensen, T.N. Palmer, F. Molteni, and F. Vitart, 2011: ECMWF seasonal forecast system 3 and its prediction of sea surface temperature. Clim, Dyn., DOI 10.1007/s00382-010-0947-3.

Su., H and J. D. Neelin., 2002: Teleconnection mechanism for tropical Pacific descent anomalies during El Niño, *J. Atmos. Sci.*, **57,** 3767-3781.

Watanabe, M., and F. F. Jin 2003: A moist linear baroclinic model: Coupled dynamical convective response to El Niño, *J Climate*, **16,** 1121-1139.

Xie, P., and P. A. Arkin, 1996, Analysis of global monthly precipitation using gauge observations, satellite estimates and numerical model predictions. *J Climate*, **9,** 840-858

Xie S –P, Annamalai H, Schott F, McCreary JP Jr, 2002: Structure and mechanisms of South Indian Ocean climate variability. *J Climate*, **15,** 864-87.